ELSEVIER

Journal of Organometallic Chemistry 545–546 (1997) 531–541

Journal of Organometallic Chemistry

Di- and trinuclear complexes of palladium with a triphosphine ligand, bis(diphenylphosphinomethyl)phenylphosphine

Tomoaki Tanase *, Hiroyuki Takahata, Masaru Hasegawa, Yasuhiro Yamamoto [1]

Department of Chemistry, Faculty of Science, Toho University, Miyama 2-2-1, Funabashi, Chiba 274, Japan

Received 23 April 1997; received in revised form 20 June 1997

Abstract

Reaction of $[Pd_2(RNC)_6](PF_6)_2$ with dpmp (2 equiv.) generated dipalladium complexes, $[Pd_2(dpmp)_2(RNC)_2](PF_6)_2$ (**1**), in good yields, where R = 2,6-xylyl (Xyl) and 2,4,6-mesityl (Mes). Complex **1a** (R = Xyl) was characterized by X-ray crystallography to have a metal–metal bonded dinuclear structure (Pd–Pd = 2.607(2) Å) without bridging ligand. The dpmp ligand chelates to the metal through only the terminal phosphorus atoms. Complex **1a** in acetonitrile easily lost one isocyanide ligand and was transformed into a dpmp-bridged dipalladium complex, *anti*-$[Pd_2(\mu\text{-dpmp})_2(XylNC)](PF_6)_2 \cdot CH_3CN$ (**(2a)**CH_3CN). The dinuclear core of **2a** consists of a three- and a four-coordinate Pd atom bridged by two dpmp ligands (Pd–Pd = 2.702(1) Å). Complex **1a** was restored by treatment of **2a** with an excess of XylNC. When compound **1** was treated with zero-valent palladium complex $[Pd_3(RNC)_6]$, A-frame trinuclear complex, A-frame-$[Pd_3(\mu\text{-dpmp})_2(RNC)_2](PF_6)_2$ (**4**), was obtained. The trimer **4** was also prepared by the reaction of $[Pd_3(RNC)_8](PF_6)_2$ with dpmp (2 equiv.) via a linear dpmp-bridged trimer, linear-$[Pd_3(\mu\text{-dpmp})_2(RNC)_2](PF_6)_2$ (**3**). Complex **4a** (R = Xyl) was analyzed by X-ray crystallography to be a trinuclear A-frame structure joined by two Pd–Pd σ-bonds (Pd–Pd = 2.592(2) Å, Pd–Pd–Pd = 79.19(8)°). The two dpmp ligands doubly bridge between the three metal atoms. Whereas, complex **4** was thermally and chemically stable, complex **3a** (R = Xyl) reacted with I_2 to lead to a trinuclear Pd(II) complex, $[\{PdI_2(dpmp)\}_2PdI_2]$ (**5**), which was characterized by an X-ray analysis. The two *cis*-PdI_2(dpmp) units were joined by *trans*-PdI_2 fragment without metal–metal bonds. © 1997 Elsevier Science S.A.

Keywords: Palladium; Triphosphine; Metal–metal bond; Isocyanide

1. Introduction

Metal–metal bonded small-size clusters of platinum and palladium have been of increasing interest as minimal models for the surface of heterogeneous catalysts, structures and properties of which can be modified by varying synthetic strategy and choice of organic ligands. Extensive studies have already been performed on dinuclear Pt(I) and Pd(I) complexes bridged by bis(diphenylphosphino)methane (dppm) [1,2], with regard to the ability to coordinate small molecules via additions across the metal–metal bond. Recently studied platinum and palladium systems have shifted to trinuclear complexes in order to mimic metal surfaces and explore new catalytic behaviors which are not established by a mononuclear center. In designing coordinatively unsaturated clusters, one of the most significant problems is how to stabilize the cluster core to resist cluster fragmentation during chemical reactions, and thus, the choice of supporting ligands such as multidentate phosphines is important. The most successful trinuclear system recently studied is the 42-valence electron triplatinum complex, $[Pt_3(\mu\text{-dppm})_3(\mu^3\text{-CO})]^{2+}$, which could provide an unsaturated reaction site composed of three metal atoms, various small molecules and metal fragments being introduced to the coordinatively unsaturated Pt_3 triangular face [3–16].

We have systematically prepared and characterized metal–metal bonded di- and trinuclear platinum and palladium complexes supported by bidentate phosphine ligands [17–23]. Recently, the tridentate phosphine ligand, bis(diphenylphosphinomethyl)phenylphosphine (dpmp), has attracted our attention because the dpmp

* Corresponding author. Department of Chemistry, Faculty of Science, Nara Women's University, Kitauoya-higashi-machi, Nara 630, Japan.

[1] Also corresponding author.

PII S0022-328X(97)00379-3

ligand has versatile bridging and chelating coordination behaviors for di- and trinuclear metal centers [24–35]. Chemistry on linearly-ordered rhodium and iridium complexes with dpmp and dpma (bis(diphenylphosphinomethyl)phenylarsine) has systematically been studied by Guimerans et al. [24], Olmstead et al. [25], Balch et al. [26–31,33,34], Olmstead et al. [32], and Balch [35], whereas the corresponding chemistry of Pt and Pd has been largely unexplored. We have recently demonstrated that the reaction of $[Pt_2(XyINC)_6]^{2+}$ (Xyl = 2,6-dimethylphenyl) with 2 equiv. of dpmp afforded a mixture of isomeric diplatinum complexes, *syn*- and *anti*-$[Pt_2(\mu\text{-dpmp})_2(XylNC)_2]^{2+}$ (*syn*-**I**, *anti*-**II**), where the central P atoms of dpmp ligands bind to the same metal center in the *syn* form and to the different metal centers in the *anti* form (Scheme 1) [36]. Complexes **I** and **II** are fluxional in solution via the symmetrical structures **I′** and **II′**. Further, the *syn*-type dimer was readily transformed, by treatment with d^{10} $M(XylNC)_2$ fragments and d^8 metal species $[MCl_2(cod)]$, to novel linear homo- and hetero-trinuclear clusters, linear-$[Pt_2M(\mu\text{-dpmp})_2(XylNC)_2]^{2+}$ (M = Pt, Pd) [36] and dimer–monomer combined complexes, $[PtMCl_2(\mu\text{-dpmp})_2(XylNC)_2]^{2+}$ [37] (Scheme 1). We wish to describe herein the synthesis and characterization of di- and trinuclear palladium complexes with the triphosphine dpmp ligand. Preliminary results have already been reported [36,38].

2. Experimental

Dichloromethane, *n*-hexane, acetone, and acetonitrile were distilled over calcium hydride and diethyl ether over lithium aluminum hydride prior to use. Other reagents were of the best commercial grade and were used as received. Complexes $[Pd_2(RNC)_6](PF_6)_2$, $[Pd_3(RNC)_8](PF_6)_2$ [18], and $[Pd_3(RNC)_6]$ [39] (R = 2,6-xylyl (Xyl) and 2,4,6-mesityl (Mes)) were prepared by the methods already reported. All reactions were carried out under a nitrogen atmosphere with standard Schlenk and vacuum line techniques.

2.1. Measurements

^1H NMR spectra were measured on a Bruker AC250 instrument at 250 MHz. Chemical shifts were calibrated to tetramethylsilane as an external reference. $^{31}P\{^1H\}$ NMR spectra were recorded by the same instrument at 101 MHz, chemical shifts being calibrated to 85% H_3PO_4 as an external reference. Infrared and electronic absorption spectra were recorded with Jasco FT/IR-5300 and Ubest-30 spectrometers, respectively.

2.2. Preparation of $[Pd_2(dpmp)_2(RNC)_2](PF_6)_2$ (1)

Compounds $[Pd_2(XylNC)_6](PF_6)_2$ (500 mg, 0.388 mmol) and dpmp (393 mg, 0.775 mmol) were dissolved

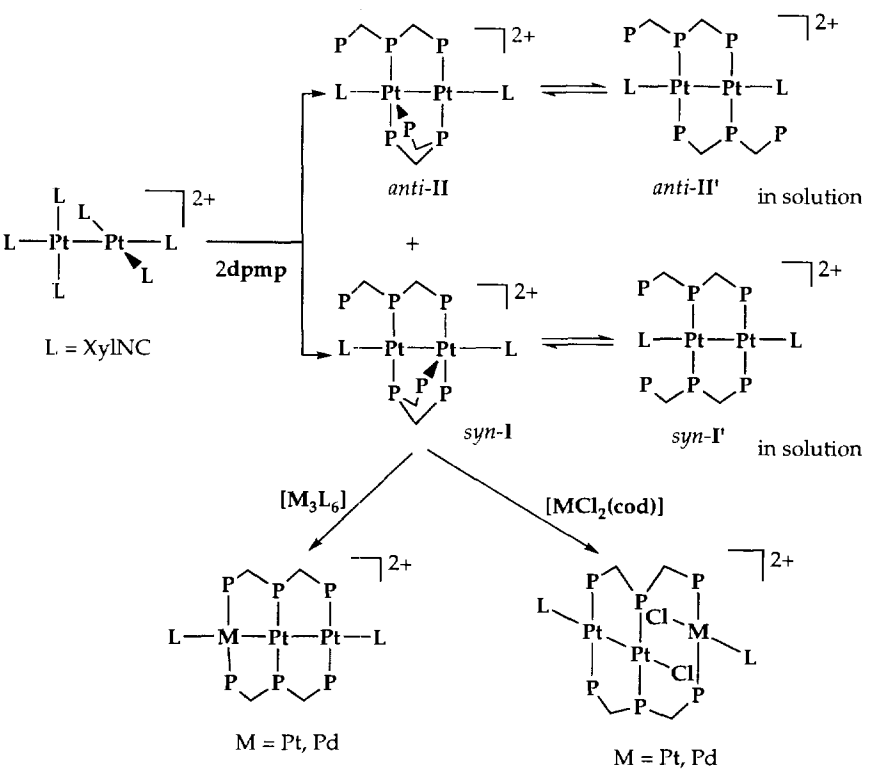

Scheme 1.

in dichloromethane (50 ml), and the solution was stirred at room temperature for 12 h. The solvent was removed under reduced pressure and the residue was crystallized from an acetone/diethyl ether mixed solvent to give yellow crystals of $[Pd_2(dpmp)_2(XylNC)_2](PF_6)_2 \cdot 3(CH_3)_2CO$ (**1a** · $3(CH_3)_2CO$) in 84% yield (566 mg). Anal Calc. for $C_{91}H_{94}N_2Pd_2P_8F_{12}O_3$: C, 55.98; H, 4.85; N, 1.43 (%). Found: C, 56.06; H, 4.79; N, 1.37 (%). IR (Nujol): 2156 (N≡C), 839 (PF_6) cm^{-1}. UV–Vis (in CH_2Cl_2): λ_{max} (log ε) 430(4.22), 274(4.43) nm. $^{31}P\{^1H\}$ NMR (in acetone-d_6): δ −38.9 (m, 2P), −5.4 (m, 2P), 12.6 (m, 2P). A slow recrystallization of **1a** · $3(CH_3)_2CO$ from an acetone/diethyl ether mixed solvent yielded block-shaped crystals of **1a** suitable for X-ray crystallography. Complex $[Pd_2(dpmp)_2(MesNC)_2](PF_6)_2 \cdot 0.5CH_2Cl_2$ (**1b** · $0.5CH_2Cl_2$) was prepared by the similar procedure using $[Pd_2(MesNC)_6](PF_6)_2$. Recrystallization of the crude product from a dichloromethane/diethyl ether mixed solvent yielded **1b** · $0.5CH_2Cl_2$ as crystalline compound in 70% yield. Anal Calc. for $C_{84.5}H_{81}N_2Pd_2P_8F_{12}Cl$: C, 54.29; H, 4.42; N, 1.52 (%). Found: C, 54.79; H, 4.16; N, 1.47 (%). IR (Nujol): 2148 (N≡C), 835 (PF_6) cm^{-1}. UV–Vis (in CH_2Cl_2): λ_{max} (log ε) 430(4.32), 273(4.58) nm. $^{31}P\{^1H\}$ NMR (in acetone-d_6): δ −42.0 (m, 2P), −8.8 (m, 2P), 8.9 (m, 2P).

2.3. Preparation of anti-$[Pd_2(\mu\text{-}dpmp)_2(xylNC)](PF_6)_2$ (2a)

Complex **1a** · $3(CH_3)_2CO$ (100 mg, 0.0562 mmol) was dissolved in 30 ml of acetonitrile and the solution was stirred at room temperature for 24 h. The solution was concentrated by reduced pressure and an addition of diethyl ether afforded dark red crystals of *anti*-$[Pd_2(\mu\text{-}dpmp)_2(XylNC)](PF_6)_2$ (**2a**) in 69% yield (64 mg). Anal Calc. for $C_{73}H_{67}NPd_2P_8F_{12}$: C, 53.24; H, 4.10; N, 0.85 (%). Found: C, 53.49; H, 3.57; N, 0.81 (%). IR (Nujol): 2162 (N≡C), 835 (PF_6) cm^{-1}. UV–Vis (in CH_2Cl_2): λ_{max} (log ε) 454(3.91) nm. ^1H NMR (in acetone-d_6): δ 1.81 (s, *o*-Me), 4.69 (br, CH_2), 7.0–7.9 (m, Ar). A slow recrystallization of **2a** from a acetonitrile/diethyl ether mixed solvent gave block-shaped crystals of (**2a**)CH_3CN which were suitable for X-ray crystallography.

2.4. Preparation of linear-$[Pd_3(\mu\text{-}dpmp)_2(xylNC)_2](PF_6)_2$ (3a)

Compounds $[Pd_3(XylNC)_8](PF_6)_2$ (308 mg, 0.186 mmol) and dpmp (227 mg, 0.449 mmol) were dissolved in dichloromethane (15 ml). After 10 min, the solution was passed through a glass filter and was concentrated to 10 ml. An addition of diethyl ether to the solution gave violet powder of *liner*-$[Pd_3(\mu\text{-}dpmp)_2(XylNC)_2](PF_6)_2$ (**3a**) (305 mg, 87%), which involved a small amount of **4a** as impurity. Anal Calc. for $C_{82}H_{76}N_2Pd_3P_8F_{12}$: C, 52.26; H, 4.06; N, 1.48 (%). Found: C, 51.95; H, 4.07; N, 1.50 (%). IR (Nujol): 2135 (N≡C), 841 (PF_6) cm^{-1}. UV–Vis (in CH_2Cl_2): λ_{max} 544, 455, 311 sh nm. Since complex **3a** was unstable in solution and easily transformed into **4a**, accurate ε was not obtained. ^1H NMR (in acetone-d_6): σ 1.67 (s, *o*-Me), 3.94–4.91 (br, CH_2), 6.8–8.0 (m, Ar). $^{31}P\{^1H\}$ NMR (in acetone-d_6): δ −15.9 (quintet, $J_{PP'} = 41$ Hz, 2P), 0.3 (triplet, $J_{PP'} = 41$ Hz, 4P).

2.5. Preparation of A-frame-$[Pd_3(\mu\text{-}dpmp)_2(RNC)_2](PF_6)_4$

$[Pd_3(XylNC)_8](PF_6)_2$ (164 mg, 0.099 mmol) and dpmp (100 mg, 0.198 mmol) were dissolved in 50 ml of dichloromethane and the solution was stirred at room temperature for 12 h. The solvent was removed under reduced pressure and the residue was extracted with acetone. The extract was concentrated and an addition of *n*-hexane gave red crystals of A-frame-$[Pd_3(\mu\text{-}dpmp)_2(XylNC)_2](PF_6)_2$ (**4a**) in 66% yield (125 mg). Anal Calc. for $C_{82}H_{76}N_2Pd_3P_8F_{12}$: C, 52.26; H, 4.06; N, 1.48 (%). Found: C, 52.22; H, 3.86; N, 1.40 (%). IR (Nujol): 2139 (N≡C), 839 (PF_6) cm^{-1}. UV–Vis (in CH_2Cl_2): λ_{max} (log ε) 471(3.59) nm. ^1H NMR (in acetone-d_6): δ 1.71 (s, *o*-Me), 4.14, 4.65, 5.39 (m, CH_2), 6.9–8.0 (m, Ar). $^{31}P\{^1H\}$ NMR (in acetone-d_6): δ −29.5 (m, $J_{PP'} = 365$ Hz, 2P), −25.5 (m, 2P), 12.9 (m, $J_{PP'} = 365$ Hz, 2P). A slow recrystallization of **4a** from a acetone/diethyl ether mixed solvent yielded blockshaped crystals of **4a** suitable for X-ray crystallography. Complex **4a** was also prepared in 49% yield by the reaction of **1a** (50 mg, 0.028 mmol) with $[Pd_3(XylNC)_6]$ (10 mg, 9.4×10^{-3} mmol) in dichloromethane and the same work-up as described above. Complex A-frame-$[Pd_3(\mu\text{-}dpmp)_2(MesNC)_2](PF_6)_2 0.5CH_2Cl_2$ (**4b** · $0.5CH_2Cl_2$) was obtained by the similar procedure by using $[Pd_3(MesNC)_8](PF_6)_2$. Crystallization from a dichloromethane/diethyl ether mixed solvent gave red crystals of **4b** · $0.5CH_2Cl_2$ in 71% yield. Anal Calc. for $C_{84.5}H_{81}N_2Pd_3P_8F_{12}Cl$: C, 52.75; H, 4.22; N, 1.46 (%). Found: C, 52.52; H, 4.12; N, 1.41 (%). IR (Nujol): 2137 (N≡C), 835 (PF_6) cm^{-1}. UV–Vis (in CH_2Cl_2): λ_{max} (log ε) 470(3.55) nm. ^1H NMR (in acetone-d_6): δ 1.76 (s, *o*-Me), 2.21 (s, *p*-Me), 4.50, 4.99, 5.73 (m, CH_2), 6.9–8.9 (m, Ar). $^{31}P\{^1H\}$ NMR (in acetone-d_6) δ −28.9 (m, $J_{PP'} = 364$ Hz, 2P), −26.4 (m, 2P), 10.6 (m, $J_{PP'} = 364$ Hz, 2P).

2.6. Preparation of $[\{PdI_2(dpmp)\}_2PdI_2]$ (5)

Complex **3a** (201 mg, 0.107 mmol) and I_2 (74 mg, 0.290 mmol) were dissolved in 10 ml of

dichloromethane and the solution was stirred at room temperature for 12 h. The reaction mixture was passed through a glass filter and was concentrated under reduced pressure. Diethyl ether was added and the solution was kept in a refrigerator to give dark red crystals of $[\{PdI_2(dpmp)\}_2PdI_2]$ (**5**) in 10% yield (10 mg). Anal Calc. for $C_{64}H_{58}Pd_3P_6I_6$: C, 37.23; H, 1.41 (%). Found: C, 37.50; H, 1.50 (%). UV–Vis (in CH_2Cl_2): λ_{max} 375 sh nm. ^1H NMR (in CD_2Cl_2): δ 3.18, 4.40 (m, CH_2), 7.1–8.0 (m, Ar). $^{31}P\{^1H\}$ NMR (in CD_2Cl_2): $\delta - 16.0$ (t, $J_{PP'} = 9$ Hz, 2P), 11.5 (d, $J_{PP'} = 9$ Hz, 4P). A slow recrystallization of **5** from a dichloromethane/diethyl ether mixed solvent yielded rectangular crystals of **5** · $4CH_2Cl_2$ suitable for X-ray crystallography.

2.7. Crystallography

The crystals used in data collection were sealed into a glass tube capillary (0.7 mm o.d.) with a droplet of mother liquor. Crystal data and experimental conditions are summarized in Table 1. All data were collected on a Rigaku AFC5S diffractometer equipped with graphite monochromated Mo Kα ($\lambda = 0.71069$ Å) radiation. The cell constants were obtained from least squares refinement of 20–25 reflections with $20 < 2\theta < 30°$. Three standard reflections were monitored every 150 reflections and showed no systematic decrease in intensity. Reflection data were corrected for Lorentz-polarization and absorption effects (ψ-scan method). The structure of **1a** was solved by Patterson method. The palladium atom was located initially, and subsequent Fourier syntheses gave the positions of other non-hydrogen atoms. The coordinates of all hydrogen atoms were calculated at ideal positions with C–H distance of 0.95 Å and were not refined. The structure was refined with the full-matrix least-square techniques minimizing $\Sigma w(|F_o| - |F_c|)^2$. Final refinement was carried out with anisotropic thermal parameters for Pd, P, and F atoms and with isotropic ones for other non-hydrogen atoms. The C(211)–C(216) atoms were treated as rigid groups of C_6H_5. The crystal structure of **1a** is low grade because the crystals are extremely delicate and quickly lost clearness in air even at low temperature. The relatively low density might indicate that some other solvent molecules still exist and are not determined in the present analysis. The structures of (**2a**)CH_3CN was solved by direct methods with MITHRIL [40]. Final full-matrix least-square refinement was carried out with

Table 1
Crystallographic and experimental data for **1a**, (**2a**)CH_3CN, **4a**, and **5** · $4CH_2Cl_2$

Compound	**1a**	(**2a**)CH_3CN	**4a**	**5** · $4CH_2Cl_2$
Formula	$C_{82}H_{76}N_2P_8F_{12}Pd_2$	$C_{75}H_{70}N_2P_8F_{12}Pd_2$	$C_{82}H_{76}N_2P_8F_{12}Pd_3$	$C_{68}H_{66}P_6Cl_8Pd_3I_6$
M	1778.09	1687.96	1884.49	2433.36
Crystal syst.	monoclinic	triclinic	monoclinic	triclinic
Space group	$C2/c$ (No. 15)	$P1-$ (No. 2)	$C2/c$ (No. 15)	$P1-$ (No. 2)
a (Å)	19.088(4)	16.420(2)	15.382(2)	13.215(5)
b (Å)	24.330(4)	16.848(3)	23.427(5))	14.497(6)
c (Å)	23.648(2)	13.542(2)	23.056(7)	11.605(7)
α (°)		90.77(1)		99.14(4)
β (°)	99.36(1)	99.97(1)	102.65(2)	107.32(5)
τ (°)		89.08(1)		76.02(5)
V (Å)	10837	3689	8107	2051
Z	4	2	4	1
T (°C)	23	23	23	23
D_{calc} (g cm^{-3})	1.090	1.519	1.544	1.970
μ (cm^{-1})	4.96	7.24	8.75	32.94
Scan method	$\omega - 2\theta$	$\omega - 2\theta$	$\omega - 2\theta$	$\omega - 2\theta$
2θ max (°)	50	45	45	45
h,k,l range	$+h, +k, \pm l$	$+h, \pm k, \pm l$	$+h, +k, \pm l$	$+h, \pm k, \pm l$
No. of data	9854	6114	5532	5380
No. of obs. data	2794 ($I > 3\sigma(I)$)	4739 ($I > 3\sigma(I)$)	2489 ($I > 2.5\sigma(I)$)	2533 ($I > 3\sigma(I)$)
Solution	Patterson method	Direct methods MITHRIL	Patterson method	Direct methods MITHRIL
No. of param.	251	537	293	412
Data/param.	11.13	8.82	8.49	6.15
R^a	0.091	0.058	0.069	0.059
R_w^a	0.074	0.045	0.063	0.059
GOF[b]	3.35	1.54	1.42	1.94
ρ_{max}, e Å^{-3}	0.91	0.83	0.76	1.04

[a] $R = \Sigma||F_o| - |F_c||/\Sigma|F_o|$; $R_w = [\Sigma w(|F_o| - |F_c|)^2/\Sigma w|F_o|^2]^{1/2}$ ($w = 1/(\sigma^2(F_o))$).
[b] GOF = $[\Sigma w(|F_o| - |F_c|)^2/(N_o - N_p)]^{1/2}$ (N_o = no. data, N_p = no. variables).

anisotropic thermal parameters for the Pd, P, F, N(1) and C(1)–C(5) atoms and with isotropic ones for other non-hydrogen atoms. The structure of **4a** was solved by Patterson method. Final refinement was carried out with anisotropic thermal parameters for the Pd, P, F, N, and C(1)–C(3) atoms and with isotropic ones for other non-hydrogen atoms. The structure of $\mathbf{5} \cdot 4CH_2Cl_2$ was solved by direct methods with MITHRIL. Final refinement was carried out with anisotropic thermal parameters for all non-hydrogen atoms.

Atomic scattering factors and values of f' and f'' for Pd, I, P, F, N, and C were taken from the literatures [41,42]. All calculations were carried out on a Digital VAX Station 3100 with the TEXSAN Program System [43]. The perspective views were drawn by using the programs ORTEP-II [44].

3. Results and discussion

Synthetic routes to di- and trinuclear palladium complexes reported in this study are summarized in Scheme 2.

3.1. Dipalladium complexes

The reaction of $[Pd_2(RNC)_6](PF_6)_2$ with 2 equiv. of dpmp readily afforded the dipalladium complexes with dpmp formulated as $[Pd_2(dpmp)_2(RNC)_2](PF_6)_2$ (**1a**: R = Xyl, **1b**: R = Mes) in high yields (70–84%). The IR spectra indicated the presence of terminal isocyanide ligands at 2148–2156 cm^{-1}. In the UV–Vis spectra, a characteristic band corresponding to σ–σ^* transition of metal–metal bond was observed around 430 nm. The energy of the band maximum is comparable to those found in $[Pd_2(diphos)_2(RNC)_2](PF_6)_2$ (diphos = *cis*-1,2-bis(diphenyl-phosphino)ethene (dppen) and $Ph_2P(CH_2)_nPPh_2$ ($n = 2$–4)) [23]. The $^{31}P\{^1H\}$ NMR spectrum of **1a** showed three multiplets at δ −38.9 (A), −5.4 (B), and 12.6 (C) in a ratio of 1:1:1, suggesting the existence of three non-equivalent phosphorus atoms (Fig. 1). From the chemical shifts, resonances B and C seemingly corresponded to phosphorus atoms coordinated to the metal and A to a phosphorus atom uncoordinated, although the coupling patterns could not be analyzed in detail. The $^{31}P\{^1H\}$ NMR spectrum of complex **1b** is similar to that of **1a**.

The structure of **1a** was determined by X-ray crystallography. An ORTEP plot of the complex cation with the atomic numbering Scheme is given in Fig. 2, and some selected bond lengths and angles are listed in Table 2. The complex cation has a crystallographically imposed C_2 symmetry and comprises two Pd(I) ions joined by a Pd–Pd σ-bond which is not supported by any bridging ligands. The Pd(1)–Pd(1)* bond length of 2.607(2) Å is comparable to those of

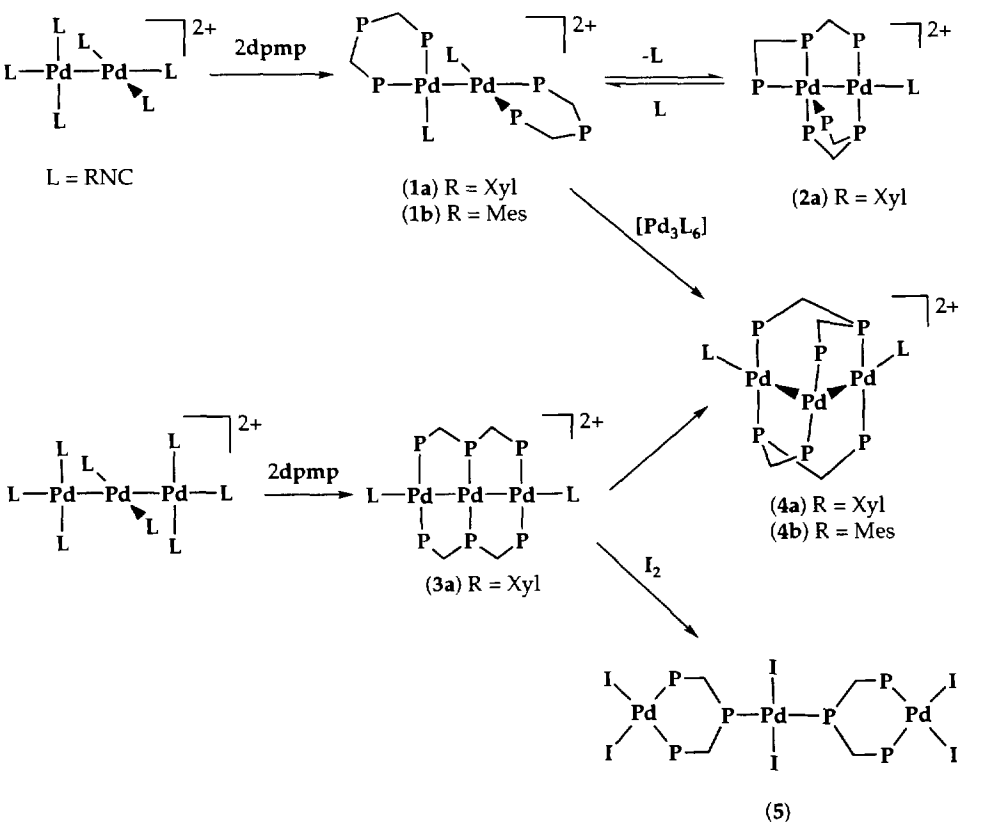

Scheme 2.

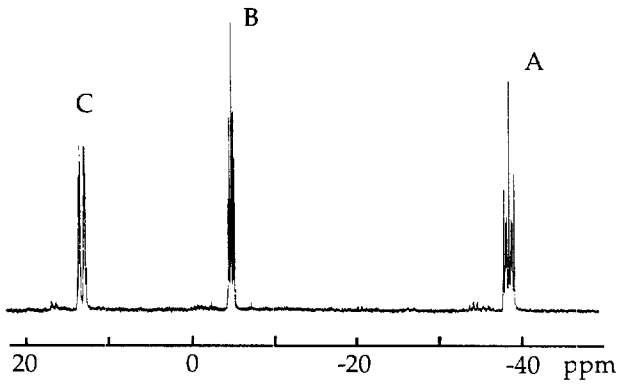

Fig. 1. $^{31}P\{^1H\}$ NMR spectrum of $[Pd_2(dpmp)_2(XylNC)_2](PF_6)_2$ (**1a**) in acetnitrile-d_3 at room temperature.

$[Pd_2(dppen)_2(XylNC)_2]^{2+}$ (2.602(1) Å) and $[Pd_2(dppp)_2(MesNC)_2]^{2+}$ (2.617(2) Å) where dppp = 1,3-bis(diphenylphosphino)propane [23]. Each palladium atom is coordinated by two phosphorus atoms of bidentate dpmp ligand, one carbon atom of terminal isocyanide, and the neighboring palladium atom in a nearly planar array. The triphosphine chelates to the metal through only the terminal P atoms and the central P atom is uncoordinated. The lone-pair electrons of the central P atoms are not directed toward the metal center. The six-membered chelate ring comprised of Pd and dpmp adopts a stable chair conformation with a *cis* angle of 97.1(2)° which is larger than that on $[Pd_2(dppp)_2(MesNC)_2]^{2+}$ (av. 94.18°) [23]. The coordination mode of dpmp in **1a** is essentially close to that observed in the mononuclear Pd(II) complex, $[PdCl_2(dpmp)]$, except for the conformation [45].

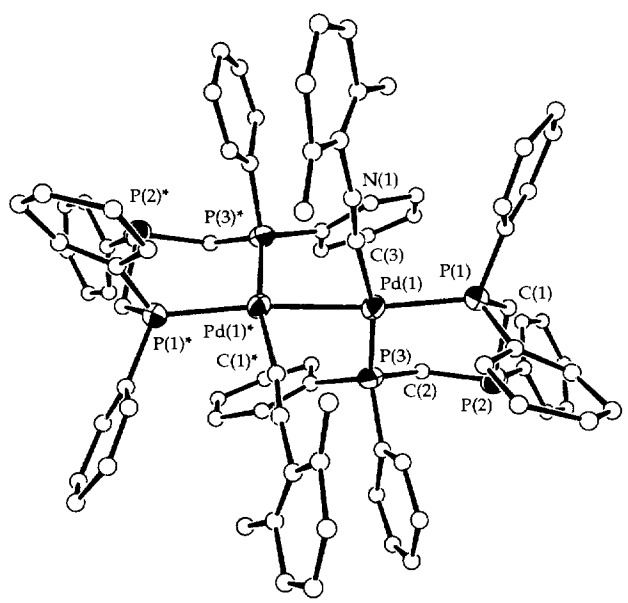

Fig. 2. ORTEP view of the complex cation of **1a**, $[Pd_2(dpmp)_2(XylNC)_2]^{2+}$. Carbon atoms are drawn by arbitrary circles and hydrogen atoms are omitted for clarity.

Table 2
Some selected bond lengths (Å) and angles (°) for $[Pd_2(dpmp)_2(XylNC)_2]$-$(PF_6)_2$ (**1a**)

Bond length			
Pd(1)–Pd(1)*	2.607(2)	Pd(1)–P(1)	2.364(4)
Pd(1)–P(3)	2.317(5)	Pd(1)–(1)	2.00(2)
N(1)–C(3)	1.17(2)	N(1)–C(11)	1.47(2)
Bond angle			
Pd(1)*–Pd(1)–P(1)	172.8(1)	Pd(1)*–Pd(1)–P(3)	90.1(1)
Pd(1)*–Pd(1)–C(1)	77.4(4)	P(1)–Pd(1)–P(3)	97.1(2)
P(1)–Pd(1)–C(3)	95.4(5)	P(3)–Pd(1)–C(1)	167.1(4)
Pd(1)–P(1)–C(1)	115.9(5)	C(1)–P(2)–C(2)	100.5(7)
Pd(1)–P(3)–C(2)	114.5(6)	Pd(1)–C(3)–N(1)	172(1)
C(1)–N(1)–C(11)	173(1)		

Unlike the diplatinum complexes of dpmp [36], the dpmp-bridged dipalladium complexes corresponding to *syn*-**I** and *anti*-**II** were not obtained and further, their existence was not observed in $^{31}P\{^1H\}$ NMR spectra of the reaction mixtures.

Complex **1a** dissolved in acetonitrile slowly lost one isocyanide ligand to lead to *anti*-$[Pd_2(\mu$-dpmp$)_2$(XylNC)$](PF_6)_2$ (**2a**), which was monitored by electronic absorption spectroscopy. The IR and ^1H NMR spectra showed the presence of one terminal isocyanide ligand, and however, the $^{31}P\{^1H\}$ NMR spectrum was composed of broad and complicated resonances for dpmp at δ $-60 \sim 10$. The electronic absorption band maximum shifted to lower energy side (λ_{max} 454 nm) compared with **1a** (λ_{max} 430 nm), suggesting that the metal–metal covalent interaction in **2a** is weaker than

Table 3
Some selected bond lengths (Å) and angles (°) of anti-$[Pd_2(\mu$-dpmp$)_2$-(XylNC)$](PF_6)_2 \cdot CH_3CN$ ((**2a**)CH_3CN)

Bond length			
Pd(1)–Pd(2)	2.702(1)	Pd(1)–P(1)	2.356(3)
Pd(1)–P(5)	2.310(3)	Pd(1)–C(5)	2.00(1)
Pd(2)–P(2)	2.272(3)	Pd(2)–P(3)	2.380(3)
Pd(2)–P(4)	2.329(3)	Pd(2)–P(6)	2.510(3)
N(1)–C(5)	1.16(1)	N(1)–C(11)	1.40(1)
Bond angle			
Pd(2)–Pd(1)–P(1)	92.63(9)	Pd(2)–Pd(1)–P(5)	79.12(9)
Pd(2)–Pd(1)–C(5)	171.0(3)	P(1)–Pd(1)–P(5)	168.1(1)
P(1)–Pd(1)–C(5)	94.3(4)	P(5)–Pd(1)–C(5)	94.8(4)
Pd(1)–Pd(2)–P(2)	85.33(9)	Pd(1)–Pd(2)–P(3)	141.49(9)
Pd(1)–Pd(2)–P(4)	78.52(8)	Pd(1)–Pd(2)–P(6)	98.35(8)
P(2)–Pd(2)–P(3)	71.5(1)	Pd(2)–Pd(2)–P(4)	155.3(1)
P(2)–Pd(2)–P(6)	105.0(1)	P(3)–Pd(2)–P(4)	110.8(1)
P(3)–Pd(2)–P(6)	116.9(1)	P(4)–Pd(2)–P(6)	95.8(1)
Pd(1)–P(1)–C(1)	113.3(4)	Pd(2)–P(2)–C(1)	110.1(4)
Pd(2)–P(2)–C(2)	96.3(4)	C(1)–P(2)–C(2)	103.5(5)
Pd(2)–P(3)–C(2)	92.2(4)	Pd(2)–P(4)–C(3)	105.7(4)
Pd(2)–P(5)–C(3)	110.2(4)	Pd(2)–P(5)–C(4)	114.3(4)
C(3)–P(5)–C(4)	105.3(5)	Pd(2)–P(6)–C(4)	103.2(3)
Pd(1)–C(5)–N(1)	172(1)	C(5)–N(1)–C(11)	177(1)

that in **1a**. The reaction of **2a** with an excess amount of XylNC regenerated complex **1a**, the transformation between **1a** and **2a** being thus reversible.

An ORTEP diagram of the complex cation of **2a** with the atomic numbering scheme is shown in Fig. 3, and some selected bond lengths and angles are listed in Table 3. The complex cation consists of three- and four-coordinate palladium atoms asymmetrically bridged by two dpmp ligands. The Pd(1) atom is ligated by one terminal isocyanide, two phosphorus atoms of dpmp ligands, and the adjacent palladium atom in a planar geometry, and the Pd(2) atom is coordinated by four phosphorus atoms of dpmp ligands and the neighboring palladium atom. The coordination geometry around the Pd(2) atom is considerably distorted and is best described as a distorted trigonal bipyramidal structure with P(2) and P(4) occupying apical sites and P(3), P(6), and Pd(1) involved in the equatorial plane. The Pd(2)–P(6) distance of 2.510(3) Å is longer than those of other P atoms (2.272(3)–2.380(3) Å), indicating that the donation from the P(6) atom to the metal center is rather weak. The Pd(1)–Pd(2) distance of 2.702(1) Å is fairly longer than that found in **1a** (2.607(2) Å) and falls within the longer end reported for Pd(I)–Pd(I) dinuclear complexes [46–52]. The value is, however, smaller than what can be found in the d^{10}–d^{10} palladium(0) dimer, $[Pd_2(Cy_2PCH_2CH_2PCy_2)_2]$ (2.7611(5) Å) [53]. From the geometrical consideration, it has tentatively resulted from a contribution of the Pd(II) and Pd(0) dative bonded structure depicted as B mixed into the Pd(I)–Pd(I) σ-bonded nature (A) (Scheme 3). Both dpmps act as bridging and chelating ligands in different ways. One dpmp ligand bridges between the two Pd atoms with a pair of terminal and central P atoms (P(1) and P(2)) and chelates to the Pd(2) atom with the other pair (P(2) and P(3)) forming a four-membered ring (P(2)–Pd(2)–P(3) 71.5(1)°). The other dpmp ligand chelates to the Pd(2)

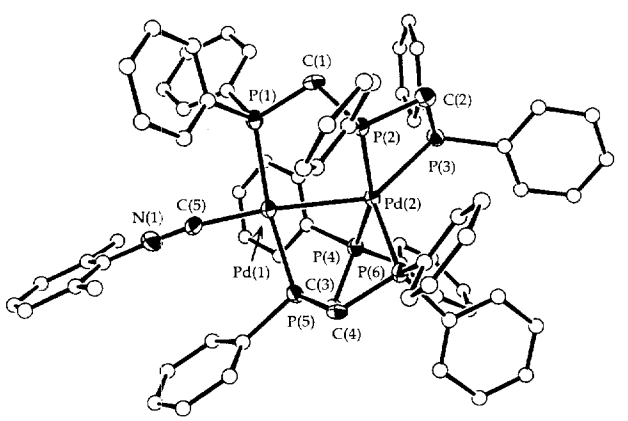

Fig. 3. ORTEP plot of the complex cation of **2a**, $[Pd_2(\mu\text{-dpmp})_2(XylNC)]^{2+}$. Carbon atoms of the phenyl and xylyl groups are drawn by arbitrary circles and hydrogen atoms are omitted for clarity.

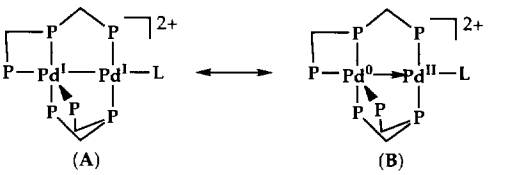

Scheme 3.

atom with two terminal P atoms (P(4) and P(6)), forming a boat conformation of a six-membered ring, and bridged to the Pd(1) atom through the central P atom (P(5)). The former coordination mode was observed in $[PtIr(CO)Cl(\mu\text{-dpmp})_2]^{2+}$ [54] and $[PdIr(CO)Cl(\mu\text{-dpmp})_2]^{2+}$ [54] and the latter in $[Re_2Cl_3(\mu\text{-dpmp})_2]^{+}$ [55]. Since the two central P atoms attach to the different metal center, we denoted this bis-dpmp bridging structure as *anti*-form. Dipalladium complexes with *syn*-structure were not obtained at all. On the basis of the structures of *anti*-$[Pt_2(\mu\text{-dpmp})_2(XylNC)_2]^{2+}$ (*anti*-**II**), complex **2a** was assumed to be formed through an intermediate complex, *anti*-$[Pd_2(\mu\text{-dpmp})_2(XylNC)_2]^{2+}$ (*anti*-**1a'** and *anti*-**1a**) (Scheme 4).

3.2. Tripalladium complexes

When $[Pd_3(RNC)_8](PF_6)_2$ was treated with 2 equiv. of dpmp, the color of the solution immediately changed to violet, and further gradually turned to dark red. From the initial violet solution, a violet complex formulated as linear-$[Pd_3(\mu\text{-dpmp})_2(RNC)_2](PF_6)_2$ (**3a**: R = Xyl) was isolated in 85% yield. The IR and ^1H NMR spectra indicated the presence of one kind of terminal iso-

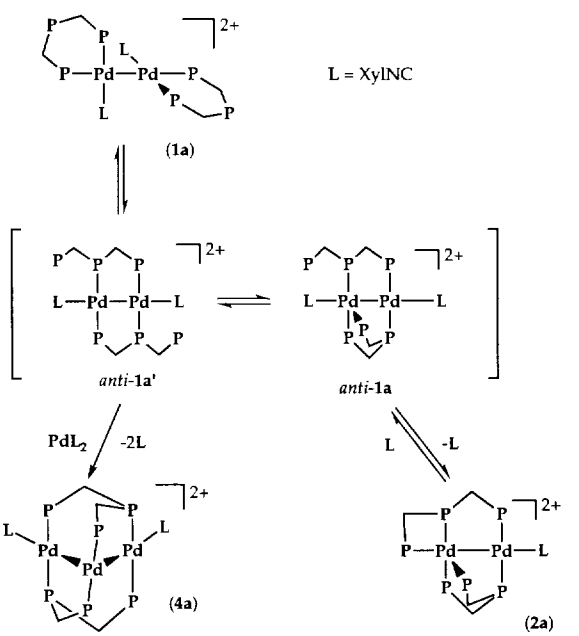

Scheme 4.

cyanide, and the UV–Vis absorption spectrum exhibited a characteristic band centered at 544 nm. The $^{31}P\{^1H\}$ NMR spectrum was simple and consisted of two resonances, a quintet at -15.9 ppm and a triplet at 0.3 ppm with $J_{PP'} = 41$ Hz, in a ratio of 1:2 (Fig. 4a). This spectral pattern is quite close to that of the linear triplatinum complex, linear-$[Pt_3(\mu\text{-dpmp})_2(XylNC)_2]^{2+}$ [36]. From the final dark red solution, red crystals of the same formula, A-frame-$[Pd_3(\mu\text{-dpmp})_2(RNC)_2](PF_6)_2$ (**4a**: R = Xyl, **4b**: R = Mes), were isolated in good yields. Whereas the IR and ^1H NMR spectra also showed one kind of terminal isocyanide, the $^{31}P\{^1H\}$ NMR spectra was entirely different from that of **3a**. In the $^{31}P\{^1H\}$ NMR spectrum of **4a** (Fig. 4b), three multiplets were observed at δ -29.5 (A), -25.5(B), and 12.9 (C) with 1:1:1 ratio. The resonances A and C largely coupled to each other with $J_{PP'} = 365$ Hz resulting in two doublets of multiplets. The large PP′ coupling suggested a *trans*-PdPP′ configuration to be involved in the structure of **4a**. In the electronic absorption spectrum of **4a**, the band at 544 nm disappeared and instead, a new band centered at 471 nm appeared.

The structure of **4a** was determined by an X-ray crystallographic analysis. An ORTEP plot of the complex cation with the atomic numbering scheme is illustrated in Fig. 5. Some selected bond distances and angles are listed in Table 4. A crystallographic C_2 axis passes at the central palladium atom along the Pd_3 plane. The complex cation involves three palladium atoms joined by two metal–metal bonds. The Pd_3 core was bridged by two dpmp ligands and terminally coordinated by two isocyanide ligands, resulting in a so-called A-frame trinuclear structure. The Pd(1)–Pd(2) distance and the Pd(2)–Pd(2)* separation are 2.592(2) Å and 3.201(3) Å, respectively. The former is slightly shorter than that of **1a** and corresponds to a Pd–Pd σ-bond, and the latter indicates the absence of metal–metal bond between the two terminal Pd atoms. The Pd(2)–Pd(1)–Pd(2)* angles is 79.19(8)°. The core

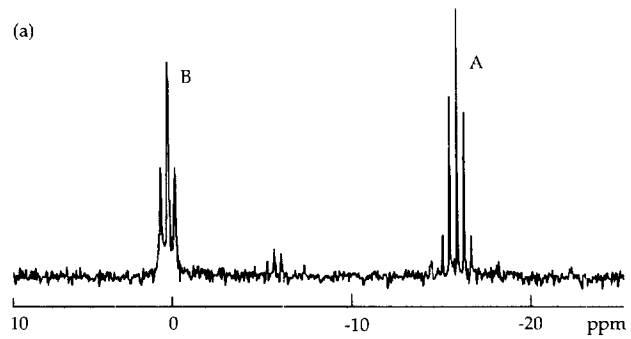

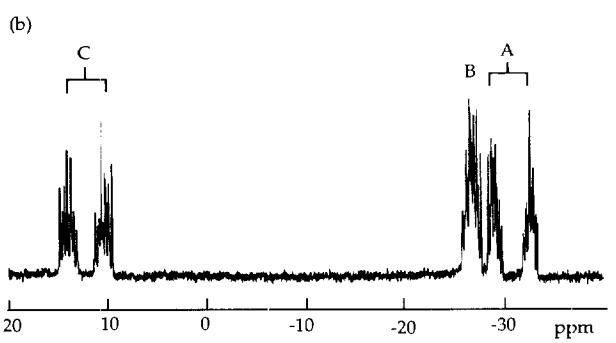

Fig. 4. $^{31}P\{^1H\}$ NMR spectra of (a) **3a** and (b) **4a** in acetone-d_6 at room temperature.

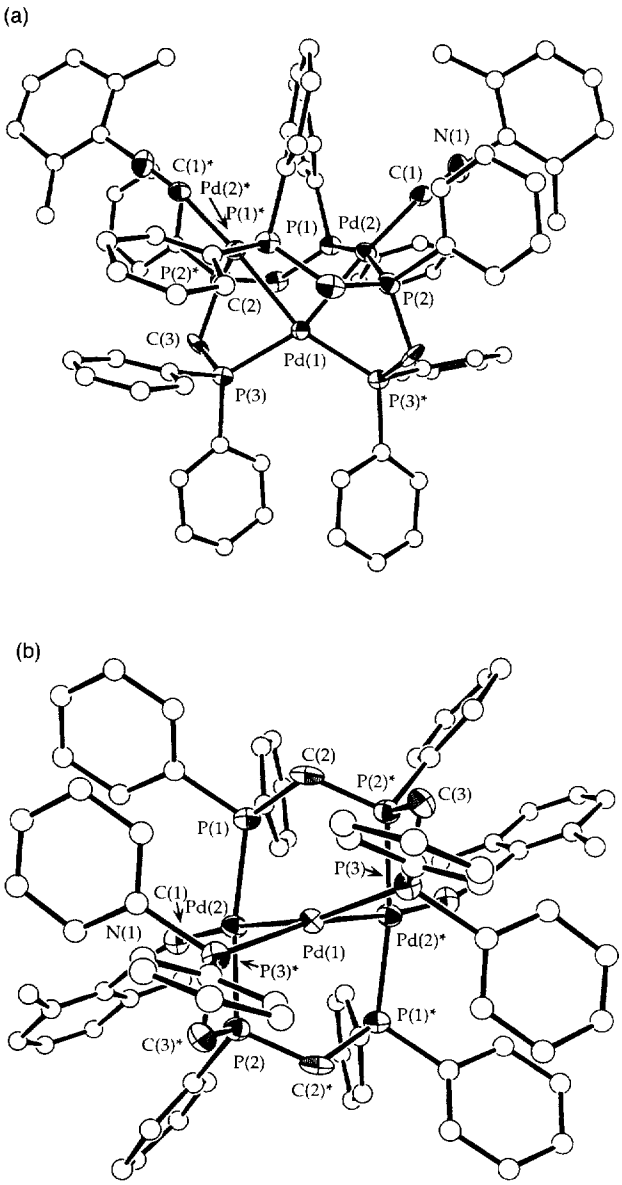

Fig. 5. ORTEP diagrams of the complex cation of **4a**, $[Pd_2(\mu\text{-dpmp})_2(XylNC)_2]^{2+}$, viewed down (a) vertical and (b) parallel to the Pd_3 plane. Carbon atoms of the phenyl and xylyl groups are drawn by arbitrary circles and hydrogen atoms are omitted for clarity.

Table 4
Some selected bond lengths (Å) and angles (°) of A-frame-$[Pd_3(\mu\text{-dpmp})_2(XylNC)_2](PF_6)_2$ (**4a**)

Bond length			
Pd(1)–Pd(2)	2.592(2)	Pd(1)–P(3)	2.300(5)
Pd(2)–P(1)	2.336(4)	Pd(2)–P(2)	2.288(5)
Pd(2)–C(1)	2.01(2)	N(1)–C(1)	1.18(2)
N(1)–C(11)	1.44(2)		
Bond angle			
Pd(2)–Pd(1)–Pd(2)*	79.19(8)	Pd(2)–Pd(1)–P(3)	158.0(1)
Pd(2)–Pd(1)–P(3)*	83.5(1)	P(3)–Pd(1)–P(3)*	116.2(2)
Pd(1)–Pd(2)–P(1)	86.6(1)	Pd(1)–Pd(2)–P(2)	76.4(1)
Pd(1)–Pd(2)–C(1)	172.8(5)	P(1)–Pd(2)–P(2)	162.8(2)
P(1)–Pd(2)–C(1)	100.3(5)	P(2)–Pd(2)–C(1)	96.6(5)
Pd(2)–P(1)–C(2)	119.3(5)	Pd(2)–P(2)–C(2)*	115.8(5)
Pd(2)–P(2)–C(3)*	109.0(5)	C(2)*–P(2)–C(3)*	104.5(8)
Pd(1)–P(3)–C(3)	101.4(5)	Pd(2)–C(1)–N(1)	165(1)
C(1)–N(1)–C(11)	171(2)		

structure is quite similar to that of $[Pt_3(\mu\text{-dppm})_2(XylNC)_2](PF_6)_2$ [17,18] except for the geometry around the central Pd atom, which is fairly distorted from a square planar structure. The dihedral angle between the [Pd(1)P(3)P(3)*] and [Pd(1)Pd(2)Pd(2)*] planes is 16.03°. The P(3)–Pd(1)–Pd(3)* angle is expanded from an ideal 90° to 116.2(2)°. The dpmp ligand bridges between the Pd(2) and Pd(2)* atoms with a pair of the outer and inner P atoms and between the Pd(1) and Pd(2) atoms with the other pair. The double bridging system of dpmp could result in the thermal stability of complex **4**.

The trinuclear A-frame complex **4a** was also obtained by the reaction of **1a** with $[Pd_3(XylNC)_6]$ which is known as a good precursor of d^{10} $Pd(XylNC)_2$ fragment. Since Hoffmann and Hoffman theoretically predicted the existence of A-frame trinuclear complexes on the basis of isolobal analogy between CH_2, and d^{10} ML_2 and d^8 ML_4 fragments [56], several synthetic examples have been prepared through insertion of metal fragments into Pd–Pd and Pt–Pt σ-bond bridged by diphosphines such as dppm (bis(diphenylphosphino)methane) and dmpm (bis(dimethylphosphino)methane). The A-frame triplatinum cluster, $[Pt_2(\mu\text{-}PtL_2)(\mu\text{-dppm})_2L_2]^{2+}$ (L = isocyanide), was prepared by the metal fragment (ML_2) insertion into the Pt–Pt bond of $[Pt_2(\mu\text{-dpmp})_2L_2]^{2+}$ [17,18], and the heterotrimetallic A-frame clusters, $[Pt_2(\mu\text{-}HgCl_2)Cl_2(\mu\text{-dppm})_2]$ [57] and $[Pt_2(\mu\text{-AuI})(C_2tBu)_2(\mu\text{-dppm})_2]$ [58], have been prepared by the reactions of the dppm-bridged diplatinum complexes with $HgCl_2$ and AuI, respectively. The reaction of $[Pd_2Cl_2(dmpm)_2]$ with $[Pt(PPh_3)_2(C_2H_4)]$ also led to the heterometallic cluster, $[Pd_2(\mu\text{-}Pt(PPh_3)_2)Cl_2(\mu\text{-dmpm})_2]$ [59]. On the basis of these examples, the formation of **4a** from **1a** can be accommodated within the context of an insertion of d^{10} ML_2 fragment into the metal–metal σ-bond. A plausible mechanism is shown in Scheme 4. Complex **1a** is transformed into the dpmp-bridged dimer *anti*-**1a'** and an insertion of $Pd(XylNC)_2$ fragment into the Pd(I)–Pd(I) σ-bond is followed by the displacement of isocyanide ligands with the terminal phosphine units. The dpmp-bridged *anti*-**1a'** is estimated to be a reactive species toward the d^{10} ML_2 fragment, since the non-bridged dipalladium(I) complex, $[Pd_2(dppp)_2(RNC)_2]^{2+}$, which has a similar structure to that of **1a**, hardly underwent the insertion of $Pd(RNC)_2$ fragment. Furthermore, the appropriately arranged uncoordinated phosphorus atoms in *anti*-**1a'** may accelerate the insertion.

3.3. Reactions of tripalladium complexes

The trinuclear A-frame complex **4** was fairly stable towards thermal, photochemical, and chemical reactions. We paid attention to the reactivity of the linear trinuclear complex **3a** next because the analogous triplatinum complex, linear-$[Pt_3(\mu\text{-dpmp})_2(XylNC)_2]^{2+}$, exhibited a versatile reactivity towards small molecules such as HBF_4, electron-deficient acetylenes, and *p*-nitrophenyl isocyanide [37]. Treatments of **3a** with HBF_4 and $MeO_2CC{\equiv}CCO_2Me$, however, resulted in the formation of **4a**, probably ascribable to the labile coordination of dpmp ligands to Pd atoms. When **3a** was reacted with an excess amount of I_2, dark red crystals formulated as $[Pd_3I_6(dpmp)_2]$ (**5**) were isolated. The N≡C stretching band disappeared in the IR spectrum. The $^{31}P\{^1H\}$ NMR spectrum simply showed a triplet at δ −16.0 and a doublet at δ 11.5 with $J_{PP'} = 9$ Hz with an intensity ratio of 1:2.

The structure of complex **5** was determined by X-ray crystallography. The unit cell contains one neutral com-

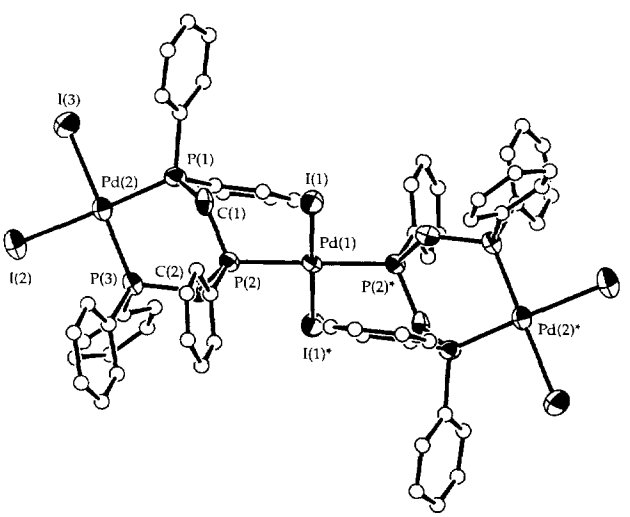

Fig. 6. ORTEP plot of $[\{PdI_2(dpmp)\}_2PdI_2]$ (**5**). Carbon atoms of the phenyl groups are drawn by arbitrary circles and hydrogen atoms are omitted for clarity.

Table 5
Some selected bond lengths (Å) and angles (°) of $[Pd_3I_6(\mu\text{-dpmp})_2]\cdot 4CH_2Cl_2$ (**5**^{a}$4CH_2Cl_2$)

Bond length			
Pd(1)–I(1)	2.613(2)	Pd(2)–I(2)	2.640(3)
Pd(2)–I(3)	2.641(3)	Pd(1)–P(2)	2.337(6)
Pd(2)–P(1)	2.253(6)	Pd(2)–P(3)	2.288(7)
Bond angle			
I(1)–Pd(1)–I(1)*	180.0	I(1)–Pd(1)–P(2)	88.2(2)
I(1)–Pd(1)–P(2)*	91.8(2)	P(2)–Pd(1)–Pd(2)*	180.0
I(2)–Pd(2)–I(3)	89.4(1)	I(2)–Pd(2)–P(1)	175.5(2)
I(2)–Pd(2)–P(3)	89.2(2)	I(3)–Pd(2)–P(1)	90.4(2)
I(3)–Pd(2)–P(3)	169.9(2)	P(1)–Pd(2)–P(3)	91.8(2)
Pd(2)–P(1)–C(1)	112.1(7)	Pd(1)–P(2)–C(1)	112.8(7)
Pd(1)–P(2)–C(2)	117.5(7)	C(1)–P(2)–C(2)	104.3(9)
Pd(2)–P(3)–C(2)	118.5(7)		

plex molecule and four solvent dichloromethane molecules. An ORTEP plot with the atomic numbering scheme is given in Fig. 6, and selected bond lengths and angles are summarized in Table 5. The complex **5** has a crystallographically imposed inversion center on the central palladium atom (Pd(1)). Two *cis*-PdI_2(dpmp) units are joined by a *trans*-PdI_2 fragment to produce a dpmp-spanned trinuclear Pd(II) structure. The six-membered ring involving the dpmp and the Pd(2) atom takes a symmetric skew-boat conformation and the bite angle is 91.8(2)° which is much smaller than that found in **1a** (97.1(2)°) with a chair conformation and that in $[PdCl_2(dpmp)]$ (99.3°) [45] with a boat form. The structure of **5** is identical to a predicted structure for $[Pd_3Cl_6(\mu\text{-dpmp})_2]$ by Olmstead et al. [45] and the ring conformational change to a skew-boat form upon binding a second palladium was also observed in $[(CH_3CN)PdCl_2(\mu\text{-dpmp})PdCl_2]$ [45].

Acknowledgements

This work was partially supported by a Grant-in-Aid for Scientific Research from the Ministry of Education of Japan.

References

[1] R.J. Puddephatt, Chem. Soc. Rev. 12 (1983) 99.
[2] A.L. Balch, in: L.H. Pignolet (Ed.), Homogeneous Catalysis with Metal Phosphine Complexes, Plenum, New York, 1983, p. 167.
[3] R.J. Puddephatt, L. Manojlovic-Muir, K.W. Muir, Polyhedron 9 (1990) 2767, and references cited therein.
[4] N.C. Payne, R. Ramachandran, G. Schoettel, J.J. Vittal, R.J. Puddephatt, Inorg. Chem. 30 (1991) 4048.
[5] M.C. Jennings, G. Schoettel, S. Roy, R.J. Puddephatt, Organometallics 10 (1991) 580.
[6] J. Xiao, J.J. Vittal, R.J. Puddephatt, J. Am. Chem. Soc. 115 (1993) 7882.
[7] J. Xiao, R.J. Puddephatt, J. Am. Chem. Soc. 116 (1994) 1129.
[8] J. Xiao, L. Hao, R.J. Puddephatt, Organometallics 14 (1995) 2194.
[9] L. Hao, I.R. Jobe, J.J. Vittal, R.J. Puddephatt, Organometallics 14 (1995) 2781.
[10] J. Xiao, L. Hao, R.J. Puddephatt, L. Manojlovic-Muir, K.W. Muir, A. Torabi, Organometallics 14 (1995) 4183.
[11] J. Xiao, L. Hao, R.J. Puddephatt, L. Manojlovic-Muir, K.W. Muir, J. Am. Chem. Soc. 117 (1995) 6316.
[12] L. Hao, J. Xiao, J.J. Vittal, R.J. Puddephatt, Angew. Chem., Int. Ed. Engl. 34 (1995) 346.
[13] L. Hao, J. Xiao, J.J. Vittal, R.J. Puddephatt, L. ManojlovicMuir, K.W. Muir, A. Torabi, Inorg. Chem. 35 (1996) 658.
[14] L. Hao, J. Xiao, J.J. Vittal, R.J. Puddephatt, Organometallics 16 (1997) 2165.
[15] M. Rashidi, E. Kristof, J.J. Vittal, R.J. Puddephatt, Inorg. Chem. 33 (1994) 1497.
[16] M. Rashidi, J.J. Vittal, R.J. Puddephatt, J. Chem. Soc., Dalton Trans. (1994) 1283.
[17] Y. Yamamoto, K. Takahashi, H. Yamazaki, J. Am. Chem. Soc. 108 (1986) 2458.
[18] Y. Yamamoto, H. Yamazaki, Organometallics 12 (1993) 933.
[19] T. Tanase, Y. Kudo, M. Ohno, K. Kobayashi, Y. Yamamoto, Nature 344 (1990) 526.
[20] T. Tanase, H. Ukaji, Y. Kudo, M. Ohno, K. Kobayashi, Y. Yamamoto, Organometallics 13 (1994) 1301.
[21] T. Tanase, Y. Yamamoto, R.J. Puddephatt, Organometallics 15 (1996) 1502.
[22] T. Tanase, T. Horiuchi, Y. Yamamoto, K. Kobayashi, J. Organomet. Chem. 440 (1992) 1.
[23] T. Tanase, K. Kawahara, H. Ukaji, K. Kobayashi, H. Yamazaki, Y. Yamamoto, Inorg. Chem. 32 (1993) 3682.
[24] R.R. Guimerans, M.M. Olmstead, A.L. Balch, J. Am. Chem. Soc. 105 (1983) 1677.
[25] M.M. Olmstead, R.R. Guimerans, A.L. Balch, Inorg. Chem. 22 (1983) 2473.
[26] A.L. Balch, R.R. Guimerans, M.M. Olmstead, J. Organomet. Chem. 268 (1984) C38.
[27] A.L. Balch, L.A. Fossett, R.R. Guimerans, M.M. Olmstead, Organometallics 4 (1985) 781.
[28] A.L. Balch, J.C. Linehan, M.M. Olmstead, Inorg. Chem. 25 (1986) 3937.
[29] A.L. Balch, L.A. Fossett, M.M. Olmstead, Organometallics 6 (1987) 1827.
[30] A.L. Balch, B.J. Davis, M.M. Olmstead, Inorg. Chem. 29 (1990) 3066.
[31] A.L. Balch, R.R. Guimerans, J. Linehan, Inorg. Chem. 24 (1985) 290.
[32] M.M. Olmstead, R.R. Guimerans, J.P. Farr, A.L. Balch, Inorg. Chim. Acta 75 (1983) 199.
[33] A.L. Balch, L.A. Fossett, J. Linehan, M.M. Olmstead, Organometallics 5 (1990) 1638.
[34] A.L. Balch, L.A. Fossett, R.R. Guimerans, M.M. Olmstead, P.E. Reedy Jr., Inorg. Chem. 25 (1986) 1397.
[35] A.L. Balch, in: S.J. Lippard (Ed.), Progress in Inorganic Chemistry, Vol. 41, 1994, p. 239, and references cited therein.
[36] Y. Yamamoto, T. Tanase, H. Ukaji, M. Hasegawa, T. Igoshi, K. Yoshimura, J. Organomet. Chem. 498 (1995) C23.
[37] T. Tanase, H. Ukaji, T. Igoshi, Y. Yamamoto, Inorg. Chem. 35 (1996) 4114.
[38] T. Tanase, H. Takahata, H. Ukaji, M. Hasegawa, Y. Yamamoto, J. Organomet. Chem., in press.
[39] F.G.A. Stone, J. Chem. Soc., Chem. Commun. (1983) 3.
[40] G.J. Gilmore, J. Appl. Crystallogr. 17 (1984) 42.
[41] D.T. Cromer, J.T. Waber, in: International Tables for X-ray Crystallography, Vol. IV, Kynoch Press, Birmingham, England, 1974.

[42] D.T. Cromer, Acta Crystallogr. 18 (1965) 17.
[43] TEXSAN Structure Analysis Package, Molecular Structure, The Woodlands, TX, 1985.
[44] C.K. Johnson, ORTEP-II, Oak Ridge National Laboratory, Oak Ridge, TN, 1976.
[45] M.M. Olmstead, R.R. Guimerans, J.P. Farr, A.L. Balch, Inorg. Chim. Acta 75 (1983) 199.
[46] T. Tanase, H. Ukaji, Y. Yamamoto, J. Chem. Soc., Dalton Trans. (1996) 3059, and references cited therein.
[47] W. Lin, S.R. Wilson, G.S. Girolami, Inorg. Chem. 33 (1994) 2265, and references cited therein.
[48] D.L. DuBios, A. Miedaner, C. Haltiwanger, J. Am. Chem. Soc. 113 (1991) 8753.
[49] K. Tani, S. Nakamura, T. Yamagata, Y. Kataoka, Inorg. Chem. 32 (1993) 5398.
[50] S. Ogoshi, K. Tsutsumi, M. Ooi, H. Kurosawa, J. Am. Chem. Soc. 117 (1995) 10415.
[51] H. Kurosawa, K. Hirako, S. Natsume, S. Ogoshi, N. Kanehisa, Y. Kai, S. Sasaki, K. Takeuchi, Organometallics 15 (1996) 2089.
[52] T. Murahashi, N. Kanehisa, Y. Kai, T. Otani, H. Kurosawa, J. Chem. Soc., Chem. Commun. (1996) 825.
[53] Y. Pan, J.T. Mague, M.J. Fink, J. Am. Chem. Soc. 115 (1993) 3842.
[54] A.L. Balch, V.J. Catalano, Inorg. Chem. 31 (1992) 2569.
[55] F.A. Cotton, M. Matusz, Inorg. Chem. 26 (1987) 984.
[56] D.M. Hoffman, R. Hoffmann, Inorg. Chem. 20 (1981) 3543.
[57] R.R. Sharp, Inorg. Chem. 25 (1986) 4185.
[58] L. Manojlovic-Muir, K.W. Muir, I. Treurnicht, R.J. Puddephatt, Inorg. Chem. 26 (1987) 2418.
[59] J. Ni, C.P. Kubiak, Inorg. Chim. Acta 127 (1987) L37.